Water Supply

IWA PUBLISHING

Water Supply Vol 22 No 3, 3242 doi: 10.2166/ws.2021.405

Numerical simulation of the effects of sandy water on regulator labyrinth channel in micro-sprinkler systems

Lin Hua[a], Hong Li[a,*], Chao Chen[a], Yue Jiang[a] and Zhonghua Zhang[b]

[a] Research Center of Fluid Machinery Engineering and Technology, Jiangsu University, Zhenjiang, Jiangsu 212013, China
[b] Research Center of Water Saving Irrigation Engineering Technology of Shanghai Jinshan, Shanghai 201505, China
*Corresponding author. E-mail: hli@ujs.edu.cn

ABSTRACT

The effects of sandy water on the W-shaped labyrinth channel of micro-sprinkler irrigation systems with large flowrate were investigated using Computational Fluid Dynamics (CFD). Using ANSYS FLUENT software and different inflow conditions (e.g., pressure, velocity, sediment concentration, and sand particle diameter), internal turbulent multiphase flow and sand deposition were simulated by the Eulerian multiphase flow model. Particle erosion in the labyrinth channel was calculated by the Discrete Phase Model (DPM). The results show that vortex movements and shear actions at the boundary layer cause self-flushing in the channel. The location of sand particle deposits and the turbulent dissipation rate are related to the operating pressure, which is optimal at 300 kPa. The erosion rate of the channel wall is proportional to the inflow sediment concentration but has no obvious relationship with inflow velocity. Based on the movement regulation of sand particles in the labyrinth channel, recommendations on filtration requirements and operating pressure of irrigation systems are proposed.

Key words: DPM, labyrinth channel, micro-sprinkler irrigator, multiphase flow simulation, sand deposition and erosion

HIGHLIGHTS

- Sand deposition in the W-shaped labyrinth channel is simulated with the Eulerian model.
- There exists an optimal pressure to control the sands deposit location.
- Particle erosion in the channel is simulated with Discrete Phase Model.
- Erosion rate of sand particles is proportional to the sediment concentration.

GRAPHICAL ABSTRACT

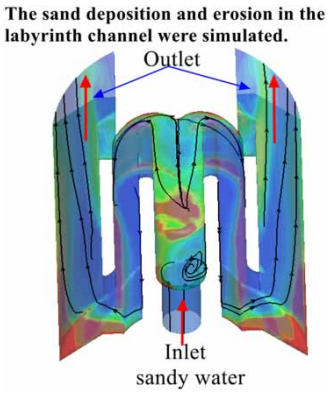

1. INTRODUCTION

In a micro-sprinkler irrigation system, laying branch pipes may result in considerable hydraulic loss and pressure differences. This phenomenon causes crops at different locations in the pipeline to receive different amounts of water and nutrients,

affecting both the overall yield and quality of crops (Martin *et al.* 2007). To alleviate this problem, pressure-compensated micro-sprinkler irrigators are commonly applied to maintain a consistent flow rate within the required range of operating pressures. This pressure compensation function is mainly achieved by a labyrinth channel and deformation of the elastic gasket inside the pressure compensation chamber. In the labyrinth channel, the movement and deposition of impurities are important factors affecting the stability of the irrigator. For example, in the fertigation system, adhesion and accumulation of incompletely melted grain-fertilizer inside the channel cause blockage and corrosion, which affect the efficiency of the irrigator (Zhai *et al.* 1999). Therefore, the flow characteristics of impurities in the irrigator channel need to be studied.

Anti-clogging performance is an important factor for evaluating the performance of irrigators. In a micro-irrigation system, the channel size of the irrigator is usually small. Due to the diversity of irrigation water sources, irrigation water contains many suspended solid particles, which increase the possibility for occurrence of emitter blockage (Nakayama & Bucks 1991). Li *et al.* (2008) simulated the turbulence and velocity distribution within labyrinth emitters and found that the smooth arc connection of flow paths enhances the self-cleaning ability of channels. Zhangzhong *et al.* (2015) analyzed the internal flow field of non-compensating emitters, and showed that the shape of the low-speed region changes with changing pressure, which affects the hydraulic characteristics of the emitter. Therefore, the flow field of the irrigator must be studied under different working pressures. Liu & Huang (2009) showed that a large flow emitter achieved better anti-clogging performance than a small flow emitter under the same irrigation time. Niu *et al.* (2013) studied the relationship between muddy irrigation water and clogging of the emitter, and identified a sensitive sediment particle diameter range, which more likely causes emitter blockage. The concentration of particles smaller than 0.1 mm is a significant factor for the occurrence of blockages. Based on prior research outlined above, the physical structure of the channel, flow rate, operating pressure, and characteristics of the flowing medium in the irrigation system are key parameters that affect clogging.

Practical micro-irrigation systems are often equipped with sufficient filtering devices and backwashing operations to reduce the probability of clogging events. However, the abrasive and erosive effect of suspended particles (e.g., sand or incompletely melted fertilizer) in the flow channel is a further problem, which affects the stability of the irrigator. It is difficult to measure debris movements inside the flow channel directly. Therefore, numerical simulation is often preferred. Ge *et al.* (2009) experimentally studied the collision between sand particles and the micro-channel wall, and measured the collision coefficient to provide accurate setting conditions for simulations. Various simulation methods applied to studies of particle movements in sandy water (e.g., Zhao *et al.* 2016) established the mass transfer equation of particles based on the Diffusive Flux Model (DFM) and simulated the flow of high-concentration suspensions in a straight micro channel. Zhao *et al.* (2016) used the Discrete Element Model (DEM) to simulate the passage rate of sand particles in the labyrinth channel. Yan *et al.* (2007) used the Discrete Phase Model (DPM) to simulate the movement of suspended particles with different mass concentrations in the labyrinth channel of an emitter. The erosion of the wall caused by suspended solid particles in the multiphase flow has been assessed via DPM (Bozzini *et al.* 2003). These studies have shown that Computational Fluid Dynamics (CFD) can be used to accurately predict the impact erosion of particles on the channel wall, which is related to their impact velocity, sediment concentration, and the target material.

Monitoring and visualizing the internal flow inside the irrigator are necessary for studying the trends of internal flow and particle migration. Particle Image Velocimetry (PIV) (Santiago *et al.* 1998) and Particle Tracking Velocimetry (PTV) (Ge *et al.* 2009) can realize the visualization of the particle movement inside the emitter. The internal channel size of the emitter is too small to carry out related experiments, although the research method using an equal scale physical model developed by Roushangar *et al.* (2020) has overcome this problem. However, the followability, visibility, and uniformity (Hadad & Gurka 2013) of fluorescent particles still create challenges for an accurate description of the flow field. Using numerical simulation, Yang *et al.* (2020) achieved accurate results for the energy dissipation of turbulent kinetic energy and the internal flow velocity in the irrigator. By using numerical simulation (Niu *et al.* 2010), multiple low-velocity zones and vortex zones can be observed, which have been considered as potential reasons for energy dispassion and clogging.

The aim of this research is to study the internal sandy flow of a large-flowrate irrigator, as most of the current research is based on drip irrigation emitters. Compared to drip irrigation (flow rate <12 L/h), micro-sprinkler irrigation uses a larger flow rate (<250 L/h), which results in different flow characteristics and intense scouring behavior inside the flow channel. This study investigated the effects of sandy water on a new labyrinth channel of the micro-sprinkler irrigator. The energy dissipation, sand deposition, and channel erosion levels were analyzed for different incoming flow conditions (i.e., sandy water with different sediment concentrations and particle diameters under several operating pressure and flow rate conditions). The behavior of sand movement in the channel is summarized, and optimal pressure and filtering requirements in the micro-

sprinkler irrigation system are proposed. These results provide additional reference for the stable operation of micro-sprinkler irrigation systems.

2. METHODOLOGY

2.1. Physical model

The modeled geometry for this simulation is based on the channel structure of a pressure-compensated micro-sprinkler irrigator (Shanghai Huawei Co., Ltd, Shanghai, China. Int. Cl. *A01G 25/02* (2006.01)) as shown in Figure 1(a). This pressure compensation irrigator consists of a base connected to the capillary, a pressure-compensated flow rate regulator, and a micro-sprinkler. As shown in Figure 1(b), the flow rate regulator contains a pressure compensation chamber, a labyrinth flow channel, and an elastic gasket, which is the key component enabling the pressure compensation function. The rated pressure compensation range of this regulator is 200–400 kPa. It has been proposed that the occurrence of blockages is independent of whether large-flowrate emitters have a pressure compensation function. Consequently, only the internal flow field of the labyrinth channel (a double-outlet, symmetrical W-shaped arc flow channel structure) was studied. Figure 2 shows a three-dimensional model of the labyrinth channel, constructed by NX.10.0 software, where the diameter of the inlet is 1.9 mm and the length of the channel is 14 mm.

2.2. Simulation method

2.2.1. Numerical simulation scheme and boundary conditions

Based on ANSYS Fluent 17.1 software, two simulations of sand movements in the labyrinth channel were carried out. Figure 3 shows a flowchart of the simulation process.

To study the energy dissipation and sand deposition in the channel, transient simulations of water-sand two-phase flow were carried out under different incoming flow conditions. The specific computational setups are listed in Table 1. Solid

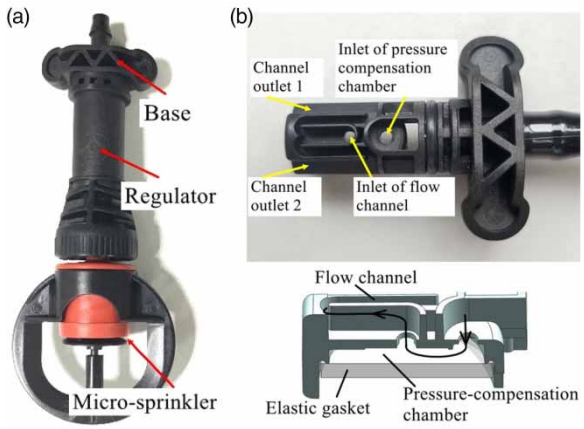

Figure 1 | Prototype of the pressure-compensating irrigator (a) and internal structure diagram of the regulator (b).

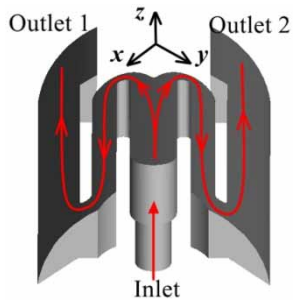

Figure 2 | Three-dimensional model of the labyrinth channel for numerical simulation.

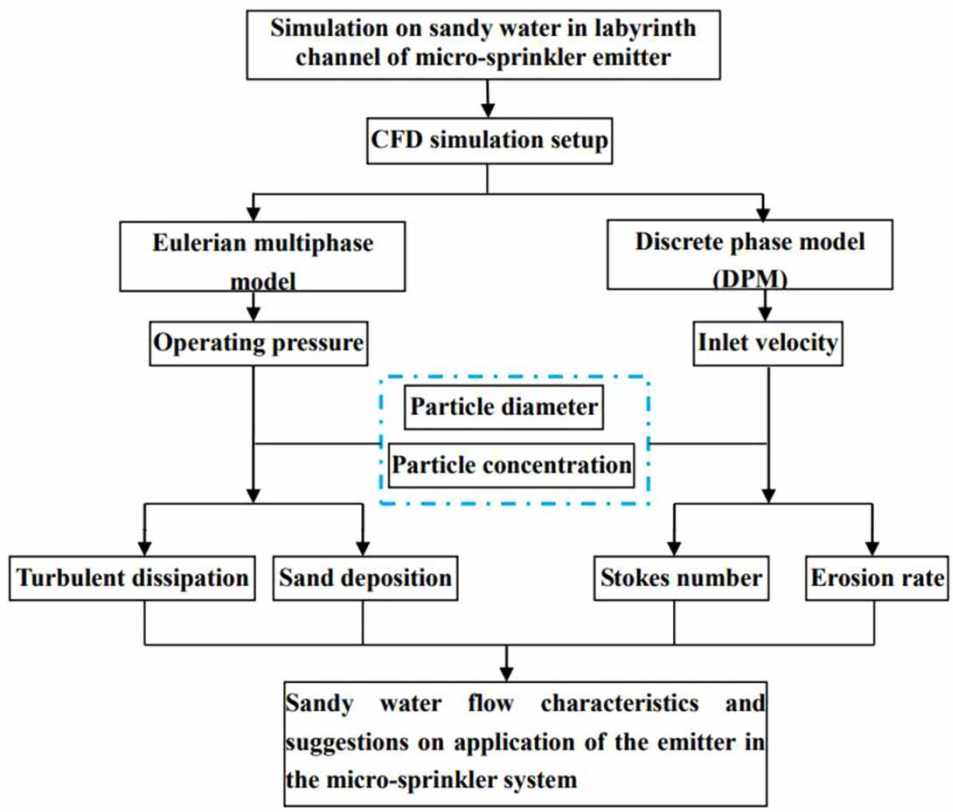

Figure 3 | Flowchart of the numerical simulation process on sandy water flow in the labyrinth channel.

Table 1 | Computational setup for the simulation of multiphase flow and discrete phase flow

	Eulerian multiphase model		Discrete phase model (DPM)	
Boundary conditions				
Inlet conditions	Pressure levels (kPa)	200/250/300/350/400	Mass flow rates of sand (10^{-4} kg/s)	1.4/1.6/1.9/2.0
	Particle diameters (mm)	0.1/0.2/0.3/0.4/0.5	Inlet diameters (mm)	1.6/1.7/1.8/1.9
	Particle concentrations (g/L)	10/20/30	Velocity (m/s)	6.9/7.3/7.6/7.8
Outlet condition	Pressure level (kPa)	0	Outflow	/
Solver control				
Convergence	Criterion	1×10^{-4}	/	/
Solver time	Transient time step (s)	5×10^{-4}	Steady iterations	2,000

particles belong to river sand with a density of 2,500 kg/m^3. The volume fraction of sand in the water remains far below 5%, indicating that the flow medium is diluted phase flow. Hence, the Eulerian Multiphase Flow model was used to simulate the deposition of sand particles in the channel. Li *et al.* (2008) found that the flow state inside the channel is turbulent, and suggested that a suitable turbulence model is required to obtain accurate numerical simulation results. Al-Muhammad *et al.* (2016) compared several turbulence models and found that the results of standard k–ε and Re-Normalization Group (RNG) k–ε models are most consistent with experimental data. Considering the turbulence anisotropy effect and the high strain rate (or the large curvature of the flow surface), the present study used RNG k–ε as viscosity model to improve the accuracy in case of swirling and large curvature. The phase coupled semi-implicit method for pressure linked equations (SIMPLE) scheme was employed for coupling between pressure and velocity. The second-order upwind scheme was

employed for spatial discretization items. The Gidaspow drag model was selected for calculating the drag force between solid phase and liquid phase.

Furthermore, to assess the sand erosion in the main flow channel, DPM was used to simulate the movement of sand particles under different inlet velocities. As the labyrinth channel stabilizes the flow rate, different flow rates can be obtained by changing the inlet diameter. Inlet velocities can be calculated according to Equation (1):

$$V = \frac{Q}{3{,}600\pi r^2} \tag{1}$$

where V is the inlet velocity (m/s), Q is the rated inlet flow rate of the irrigator (m^3/s), and r is the radius of the inlet (mm). The sediment concentration of the inlet flow is 10 g/L; that is, the mass flow rate of sand is 1% of the flow rate Q. The diameters of injected solid particles conform to the Rosin-Rammler distribution, with a range of 0.001–0.1 mm. The relationship between the particle size distribution and the mass fraction satisfies the following functional relationship:

$$Y_{\mathrm{d}} = e^{-\left(\frac{d}{\bar{d}}\right)^n} \tag{2}$$

where Y_{d} is the mass fraction, d is the particle diameter, $\bar{d}$ is the mean particle diameter (0.05 mm), and n is the spread parameter (3.5).

Particle erosion rates were monitored at wall boundaries. The erosion rate is defined by Equation (3):

$$R_{\mathrm{erosion}} = \sum_{P=1}^{N_{\mathrm{particles}}} \frac{mbC(d_{\mathrm{p}})f(\alpha)v^{b(v)}}{A_{(\mathrm{face})}} \tag{3}$$

where $C(d_{\mathrm{p}})$ is a function of the particle diameter, set to a constant of 1.8e-9, $f(\alpha)$ represents the function of impact angle, and α is the impact angle of the particles on the wall. $b(v)$ represents the function of relative particle velocity, set to a constant of 2.6 for the simulation, v is the relative velocity of the particle phase to the wall, and $A_{(\mathrm{face})}$ is the area of the cell face at the wall. According to the experimental measurement of Ge *et al.* (2009), the normal discrete phase reflection coefficient R_{cn} was set to 0.44, and the tangent discrete phase reflection coefficient R_{ct} was set to 0.83.

2.2.2. Computational grid and independent test

The simulation grids were acquired by ANSYS ICEM 17.1 software, which includes a simplified structured grid of the main channel for DPM simulation, and an unstructured grid of the whole channel for Eulerian multiphase flow simulation. To ensure calculation accuracy and reduce processor calculation cost, independent tests on the calculation mesh were performed to identify the optimal mesh. In Table 2, five types of meshes with different cell sizes were used to simulate the internal flow of channels under 200 kPa. Outlet velocity was monitored to evaluate the computational accuracy of the optimal mesh. The unstructured Mesh 4 with 3×10^5 grids and the structured Mesh 4 with 2.3×10^5 grids were selected as computational grids for numerical simulations.

Table 2 | Grid parameters for independent verification

Meshes	Total number of tetrahedral cells (10^5) (unstructured grid)	Outlet velocity (m/s)	Total number of hexahedral cells (10^5) (structured grid)	Outlet velocity of sand (m/s)
Mesh 1	0.73	4.89	0.8	3.25
Mesh 2	1.09	4.83	1.2	3.26
Mesh 3	1.77	4.85	1.7	3.32
Mesh 4	3.03	4.91	2.3	3.44
Mesh 5	5.87	4.93	3.1	3.47

3. RESULTS AND DISCUSSION

3.1. Hydraulic performance of irrigator

Figure 4 shows the general relationship between the flow rate and pressure of the irrigator. At a certain sediment concentration, flow rate values with different sand particle diameters were averaged, as the particle concentration is the main factor causing blockage at a relatively large flow rate of the irrigator (Hadad & Gurka 2013). Under the same pressure level, a greater sand concentration results in a smaller outlet flow of the regulator. The flow rate of the irrigator was tested with sandy water with a sand concentration of 10 g/L. The errors between experimental data and simulation results remain within 10%, indicating calculation accuracy of the numerical simulation. Sigma Plot 14.0 software was used for the linear regression calculation of the operating pressure and the corresponding discharge, which can be expressed by the flow rate-pressure equation as:

$$Q = kH^x \tag{4}$$

where Q represents the flow rate (L h^{-1}), and the flow coefficient k is determined by the geometric structure of the emitter flow channel. x represents the flow index, which is a decimal in the range of (0, 1), used to evaluate the hydraulic performance of the emitter (the lower this index, the better the performance of the emitter). Figure 4 shows that an increase in sediment concentration leads to an increase in the discharge coefficient and a decrease in the flow index of the irrigator. A possible reason is that the energy-consuming movements of particles in the channel, such as collision and friction, are stronger at higher concentrations. While such active movements require more energy, they enable more sensitive flow rate adjustments of the irrigator. The flow index of the general labyrinth channel is ~0.5 (Li & Li 2011) and the flow index of this irrigator is ~0.35, indicating good energy dissipation performance of the labyrinth channel structure.

Figure 5 depicts the relationship between operating pressure and turbulent kinetic energy (TKE) dissipation ratios under different conditions. Energy dissipation in the channel can be reflected by the TKE dissipation ratio, which is defined as the ratio of the difference in TKE between inlet and outlet to the inlet TKE. When the pressure is below 300 kPa, the TKE dissipation ratio remains steady at 0.75 despite pressure changes. Consequently, about 75% of the energy of the flowing medium is converted to internal energy and then dissipated. If the pressure exceeds 300 kPa, the TKE dissipation ratio gradually decreases with increasing pressure. This indicates that the TKE difference between the outlet and the inlet of the flow channel becomes small, and the energy dissipation effect of the flow channel worsens. For a constant pressure condition exceeding 300 kPa, if the concentration of sand particles increases, both the TKE dissipation ratio and the energy dissipation effect decrease. Similarly, the TKE dissipation ratio decreases significantly if the diameter of sand particles increases.

3.2. Flow characteristics in labyrinth channels

Figure 6 shows the vorticity contour in the channel at a pressure of 300 kPa. At the inlet of the flow channel, because of the restricted channel structure, the flow direction of the incoming flow abruptly changes from Z direction to X-Y direction and forms many backflows and vortices. The mixing of flows is an effective energy dissipation behavior at the inlet position.

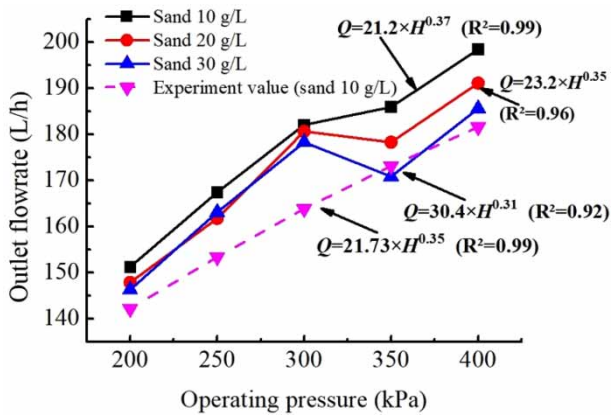

Figure 4 | Relationship between the outlet flow rate and pressure for different sand concentrations.

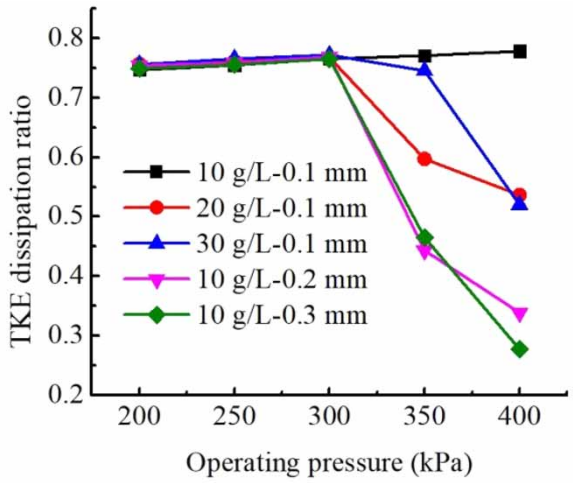

Figure 5 | Relationship between kinetic energy dissipation ratio and operating pressure.

Therefore, the vorticity value in this region is much higher than that of the surrounding area. The existence of vortices as well as the viscous stresses in the boundary layer between fluid and wall cause locally high vorticity values. For example, at curve transition sections, streamlines are smooth and without vortices. However, the vorticity here is highest at around 8–20 (10^3 s^{-1}) and water velocity reaches 10–12 m/s, implying that the flow is scouring the wall of the flow channel at high speed. Li *et al.* (2018) identified flushing of the channel as an effective way to reduce clogging. Therefore, in the flow field of the labyrinth channel, turbulent flow with high vorticity not only causes energy dissipation but also strengthens the self-washing and reduces sedimentation of sand by flushing the channel wall. Moreover, the vorticity value is proportional to the energy dissipation and inversely proportional to the sediment concentration.

3.3. Sand deposition characteristics in the labyrinth channel

Pressure is one of the important factors affecting the distribution of sand particles in the labyrinth channel. The contours of the sand phase volume fraction under different pressure conditions are compared, to assess the relationship between pressure and sand deposition. It is found that 300 kPa is the critical pressure at which the location of sand deposition changes. Figure 7(a) shows the sand distribution characteristics in the channel for pressures below 300 kPa. Sand particles are mainly settled along the outer side of the bend and the straight channel, and sand deposition is proportional to sediment concentration. At the same concentration, the sediment distribution in the channel is similar, but smaller particle sizes are more likely to cause clogging. Since these small sand particles also have lower kinetic energy, once they enter the low-velocity zone, they cannot escape, resulting in clogging. Figure 7(b) shows the sand distribution in the channel for pressures above 300 kPa, where sand particles are mainly deposited in the downstream face of the bent channel, which is completely different. At high

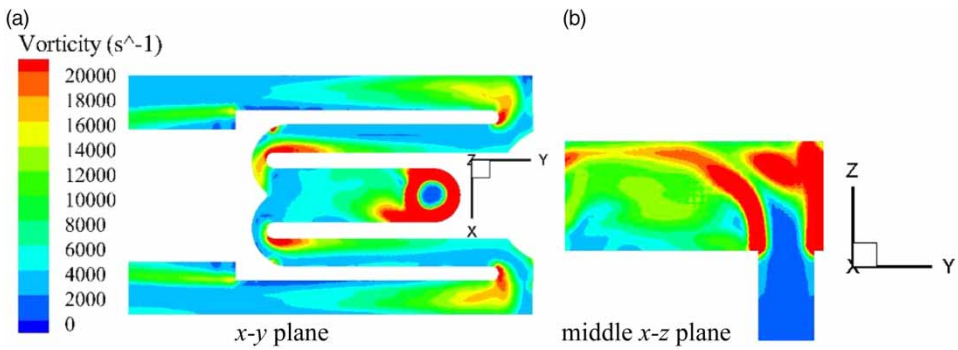

Figure 6 | Vorticity contour of the flow in the channel under 300 kPa, where the medium is sandy water with sand particle diameters of 0.3 mm at a concentration of 2 g/mL.

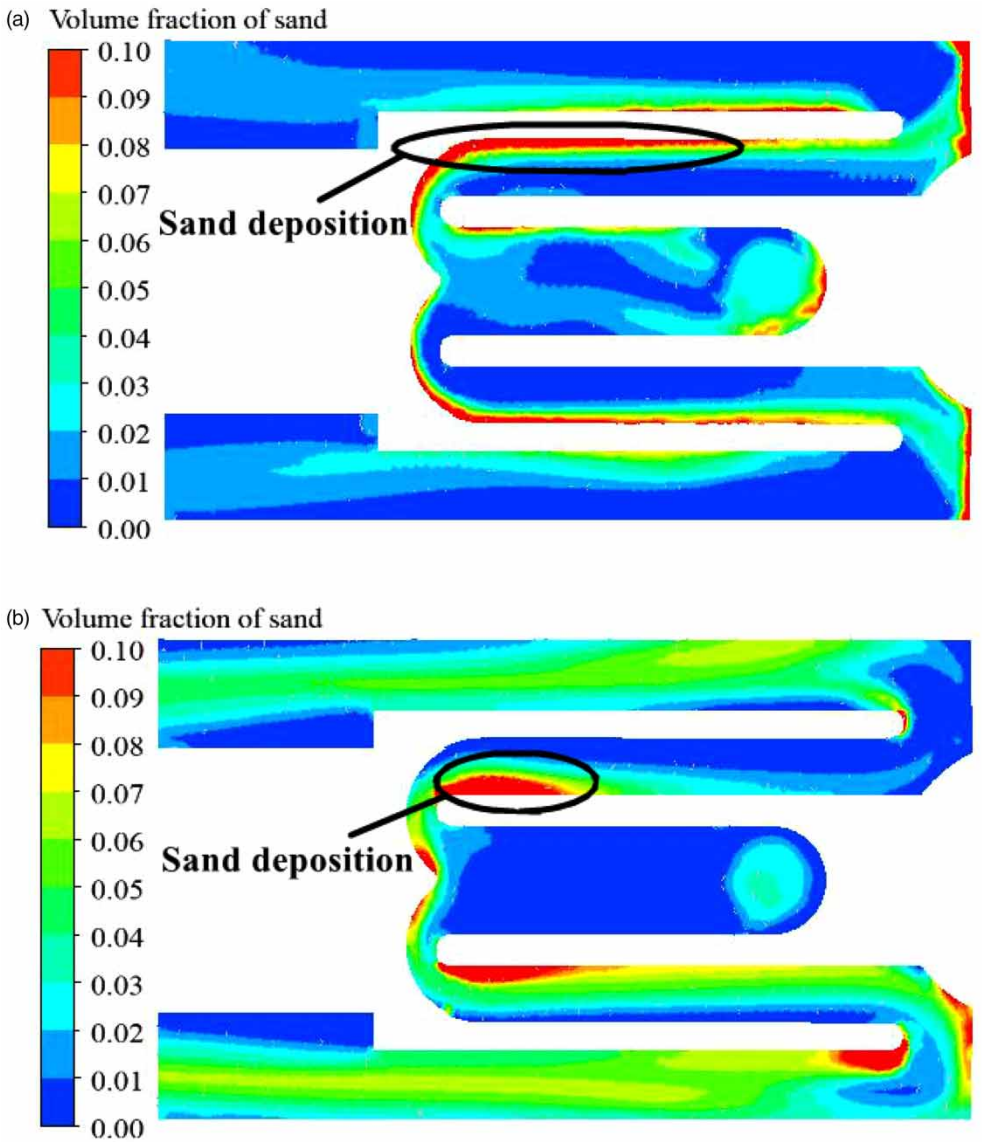

Figure 7 | Two types of volume fraction distributions of the solid phase at the bottom plane of the channel depending on operating pressure. (a) Sand deposition position sample contour for pressures below 300 kPa (the sand diameter is 0.5 mm, the sediment concentration is 30 g/L, and the operating pressure is 300 kPa). (b) Sand deposition position sample contour for pressures over 300 kPa (the sand diameter is 0.2 mm, the sediment concentration is 30 g/L, and the operating pressure is 400 kPa).

pressure levels, the kinetic energy of the flow is large. Thus, there is an obvious speed difference in the inner bend of the channel. The velocity of the upstream face exceeds that of the downstream face. Consequently, a low-velocity zone forms at the downstream face, where sand particles are deposited.

Figure 8 shows the single emitter clogging rate with different sandy water conditions under different pressures. According to the international standard, the single emitter clogging rate I can be calculated by Equation (5):

$$I = \frac{Outflow - Inflow}{Inflow} \times 100\% \tag{5}$$

As $I \geq 0.25$, blockage occurs inside the emitter flow channel. Figure 8 shows that the clogging rate I is related to the operating pressure, and 300 kPa is the critical pressure threshold, determining whether blockage occurs. If the operating pressure remains below 300 kPa, the occurrence of clogging inside the channel depends on the conditions of the incoming flow (i.e.,

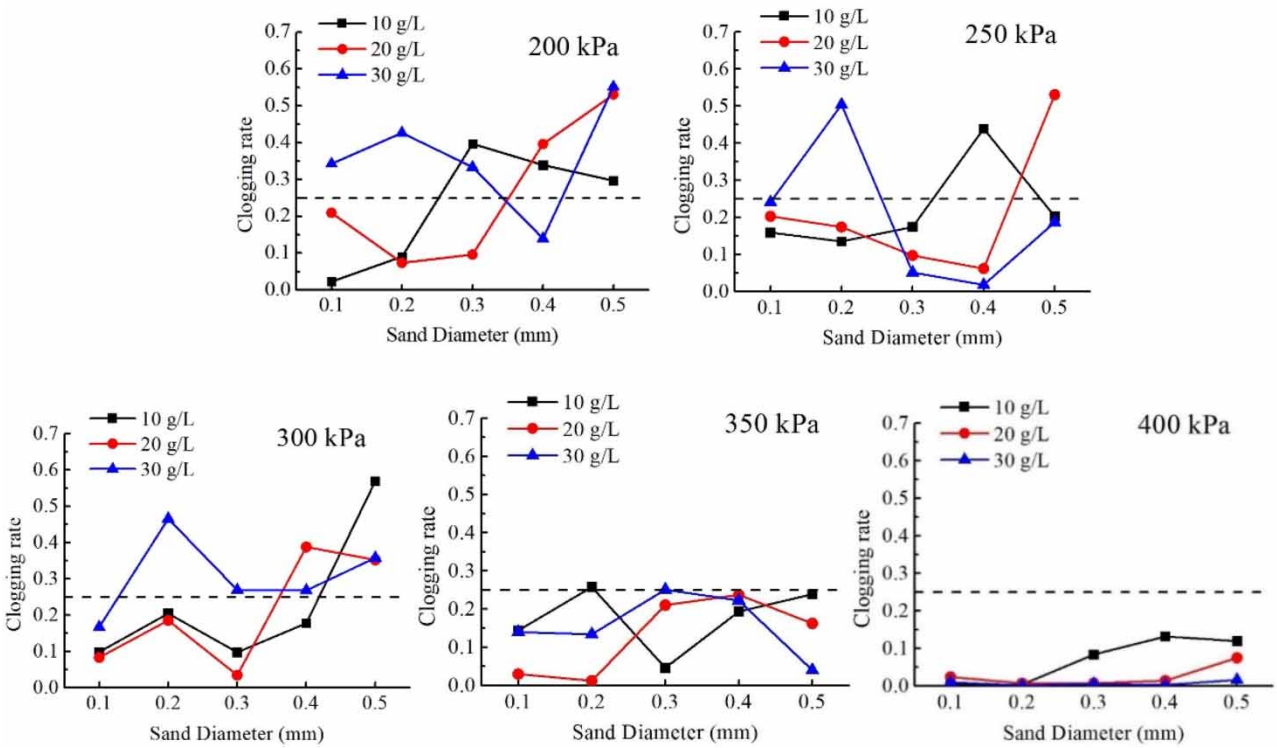

Figure 8 | Volume fraction contour of sand on the plane *x-y* in the channel.

both sediment concentration and sand diameter). If the flowing medium is sandy water with high sediment concentration, flow with smaller sand diameters achieves a higher blockage rate, and blockage is more likely to occur in the channel. The possible reason for this phenomenon is that the kinetic energy of small sand particles is weak. After entering the low-velocity region, sand particles do not have enough kinetic energy to escape. Thus, their deposition in the velocity dead zone leads to a risk of blockage. If the flowing medium is sandy water with low sediment concentration, flow with a larger sand diameter results in a greater blockage rate. The possible reason is that at low sediment concentration, small sand particles are directly washed out of the channel because of their better flow behavior, whereas large sand particles are more likely to deposit inside the channel because of gravity and collision. However, when the operating pressure exceeds 300 kPa, the clogging rates at any operating conditions remain below 0.25; that is, clogging is less likely to occur in the channel.

In summary, the location of sand accumulation in the labyrinth channel of the emitter can be obtained through numerical simulation. The probability of the blockage of a single emitter under different sandy water conditions can be calculated. The clogging rate can be used to evaluate the optimal operating pressure and the critical filtering standard of the irrigation system.

3.4. Stokes number of particles in a labyrinth channel

The track of particles in turbulent flow is related to the inertia and expansion capabilities of particles, which can be reflected by the Stokes number (Crowe *et al.* 1988). The Stokes number is proportional to the ratio of the particle aerodynamic response time (τ_A) and the fluid time (τ_F), which is expressed as:

$$S_t = \frac{\tau_A}{\tau_F} = \frac{\frac{\rho_p d_p^2}{18\mu_l}}{D/V} = \frac{\rho_p d_p^2 V}{18\mu_l D} \tag{6}$$

where ρ_p is the particle density, d_p is the particle diameter, μ_l is the liquid dynamic viscosity, V is the flow velocity, and D is the hydraulic diameter. If $S_t < 1$, particles will follow the flow very well; if $S_t \sim 1$, particles will deviate from the following trajectory; if $S_t > 1$, particles can penetrate turbulent flow structures, and the inertial force plays a dominant role in the motion of particles.

Figure 9 shows the Stokes number of the particle swarm at the inlet of the channel according to DPM simulation. The result shows that the standard deviation of the Stokes number of sand between different inlet velocity conditions is not significant; that is, remains within 0.13. If the diameter of sand particles exceeds 0.04 mm (which accounts for ~70% of the particle swarm), the Stokes number of sand exceeds 1, implying that such sand particles do not move well with the flow in the flow channel. The followability of sand particles in the fluid affects the trajectory of particles. Therefore, it can be assumed that during the flow process, the probability for collision between sand particles and channel increases with a large Stokes number. This also implies that the erosive effect of sand particles on the wall of the channel is mainly caused by sand particles with a diameter exceeding 0.04 mm.

3.5. Erosion on the wall of the labyrinth channel

In the labyrinth channel, the bend section has a direct collision with the flow, and the erosion will be more severe here than at the straight section. Therefore, DPM simulation focused on monitoring the erosion rate on the wall of the arc channel. The results are presented in Tables 3 and 4. Table 3 shows the relationship between flow velocity and erosion rate on the channel wall. These results reflect that changing the inlet velocity has less effect on the sand erosion rate. If the sand concentration is 10 g/L, the average erosion rate remains around 3.66×10^{-8} kg/m^2-s, independent of the inlet velocity. Table 4 shows an obvious proportional relationship between sediment concentration and erosion rate. With increase in sand concentration, the erosion on the channel wall increases because more solid particles collide with the channel surface. However, according to the research of Zheng *et al.* (2008), with increase in sediment concentration, the interaction between solid particles will consume considerable kinetic energy. Therefore, the erosion rate will not change significantly. To reduce erosion of the labyrinth channel surface and prolong the service life of the emitter, the concentration of impurities in the pipeline needs to be controlled, without having to adjust the operating flow rate of the micro-sprinkler irrigation system. Furthermore, the materials of the emitter should be adjusted by the corresponding water source quality to strengthen the adaptability of the emitter.

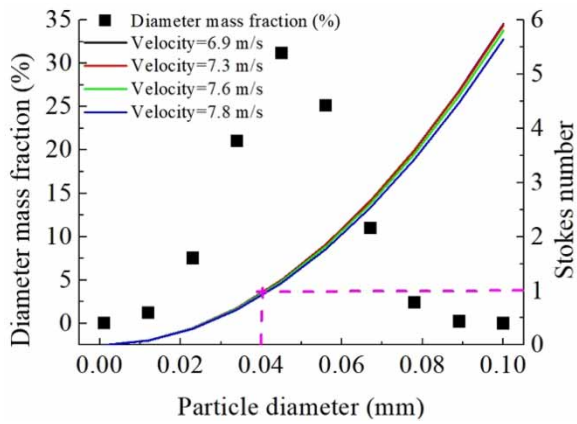

Figure 9 | Stokes number of particle swarms at the inlet of the channel, where the diameters of particles follow an R-R distribution, and the sand concentration is 10 g/L.

Table 3 | Erosion rates of the channel under different inlet velocities (at a sediment concentration of 10 g/L)

Inlet diameter (mm)	Rated inlet flow rate (L/h)	Inlet velocity (m/s)	Mass flow rate of sand particles (10^{-4} kg/s)	Average erosion rate (10^{-8} kg/m^2-s)	Maximum erosion rate (10^{-8} kg/m^2-s)
1.6	50	6.9	1.39	3.43	4.18
1.7	60	7.3	1.67	4.23	4.24
1.8	70	7.6	1.94	3.56	3.92
1.9	80	7.8	2.22	3.42	4.39

Table 4 | Erosion rates of the channel under different sediment concentrations (the inlet flow rate is 80 L/h and inlet velocity is 7.8 m/s)

Sediment concentrations (g/L)	Mass flow rate of sand particles (10^{-4} kg/s)	Average erosion rate (10^{-8} kg/m^2-s)	Maximum erosion rate (10^{-8} kg/m^2-s)
10	2.22	3.42	4.39
20	4.44	6.22	7.87
30	6.66	10.09	11.24

4. CONCLUSIONS

This study evaluated the flow characteristics of sandy water in a W-shaped labyrinth channel through CFD numerical simulation. The distribution of accumulated sand and erosion problems in the channel were investigated under different flow conditions. The simulation data show that because of the effects of the labyrinth flow channel structure on sandy water, the reflow mixing behavior and shear action inside the channel increase energy dissipation and reduce the risk of sand accumulation. The optimal operating pressure of the micro-sprinkler irrigation system is estimated from the deposition distribution and the erosion rate of sand by numerical simulation. Applying this optimal operating pressure reduces the sand deposition and erosion in the labyrinth channel while ensuring the basic hydraulic performance of the emitter. In this specific case study, the optimal operating pressure for the micro-sprinkler emitter is 300 kPa. The erosion of sand particles on the channel surface is proportional to the sediment concentration and independent of the flow velocity. Micro-sprinkler irrigation systems should formulate a relevant filtration standard of sand concentration rather than restrict the diameter of sand particles, as this reduces the configuration requirements of the filtration device and the system construction cost. The data and conclusions of this research are all drawn from numerical simulation, and corresponding experimental research may be implemented in the future to assess the actual flow conditions inside the labyrinth channel.

AUTHOR CONTRIBUTIONS

Simulation work and writing-original draft preparation, Lin Hua; funding acquisition and writing review, Hong Li, Chao Chen, and Yue Jiang; provision of the product physical model, Zhonghua Zhang.

CONFLICTS OF INTERESTS

The authors declare no conflict of interest.

FUNDING

This work was financially supported by the National Natural Science Foundation of China (grant Nos. 51939005, 51809119, and 51679109), the Postgraduate Scientific Research and Innovation Project of Jiangsu Province (grant No. KYCX21_3345), the National Key Research and Development Project of China (grant No. 2017YFD0201500), and a Project Funded by the Priority Academic Program Development of Jiangsu Higher Education Institutions (grant No. PAPD-2018-87).

DATA AVAILABILITY STATEMENT

All relevant data are included in the paper or its Supplementary Information.

REFERENCES

Al-Muhammad, J., Tomas, S. & Anselmet, F. 2016 Modeling a weak turbulent flow in a narrow and wavy channel: case of micro-irrigation. *Irrigation Science* **2016**, 361–377. doi:10.1007/s00271-016-0508-6.

Bozzini, B., Ricotti, M. E., Boniardi, M. & Mele, C. 2003 Evaluation of erosion-corrosion in multiphase flow via CFD and experimental analysis. *Wear* **255**, 237–245.

Crowe, C. T., Chung, J. N. & Troutt, T. R. 1988 Particle mixing in free shear flows. *Progress in Energy and Combustion Science* **14**, 171–194.

Ge, L., Wei, Z., Tang, Y., Wu, S. & Lu, B. 2009 Simulation and experimental analysis on sand-wall collisions in labyrinth channel emitter. *Transactions of the Chinese Society of Agricultural Machinery* **40**, 46–50.

Hadad, T. & Gurka, R. 2013 Characteristics of seeding particles for PIV/PTV analysis. *Experimental Thermal and Fluid Science* **45**, 203–213.

Li, Y., Yang, P., Xu, T., Ren, S., Lin, X., Wei, R. & Xu, H. 2008 CFD and digital particle tracking to assess flow characteristics in the labyrinth flow path of a drip irrigation emitter. *Irrigation Science* **26**, 427–438.

Li, Z. & Li, L. 2011 The influence of the sectional form of labyrinth emitter on the hydraulic properties. *Communications in Computer and Information Science* **237**, 499–505.

Li, Z., Yu, L., Li, N., Chang, L. & Cui, N. 2018 Influence of flushing velocity and flushing frequency on the service life of labyrinth-channel emitters. *Water* **10**, 1–14.

Liu, H. & Huang, G. 2009 Laboratory experiment on drip emitter clogging with fresh water and treated sewage effluent. *Agricultural Water Management* **96**, 745–756.

Martin, D. L., Heermann, D. F. & Madison, M. 2007 Hydraulics of sprinkler and microirrigation systems. In: *Hydraulics of Sprinkler and Microirrigation Systems* (McCann, P., ed). American Society of Agricultural and Biological Engineers, St. Joseph, MI, pp. 532–556.

Nakayama, F. S. & Bucks, D. A. 1991 Water quality in drip/trickle irrigation: a review. *Irrigation Science* **12**, 187–192.

Niu, W., Wu, P. & Yu, L. 2010 Anti-clogging experimental investigation and optimized design of micro-channels of emitter based on isoline of sand content. *Transactions of the CSAE* **26**, 14–20.

Niu, W., Liu, L. & Chen, X. 2013 Influence of fine particle size and concentration on the clogging of labyrinth emitters. *Irrigation Science* **31**, 545–555.

Roushangar, K., Khowr, A. F., Saniei, M. & Alizadeh, F. 2020 Investigating impact of converging training walls of the ogee spillways on hydraulic performance. *Paddy and Water Environment* **18**, 355–366.

Santiago, J. G., Wereley, S. T., Meinhart, C. D., Beebe, D. J. & Adrian, R. J. 1998 A particle image velocimetry system for microfluidics. *Experiments in Fluids* **25**, 316–319.

Yan, D., Yang, P. & Ren, S. 2007 Study on dynamic analysis of particle movement in drip emitter based on CFD. *Transactions of the Chinese Society for Agricultural Machinery* **38**, 71–74.

Yang, B., Wang, J., Zhang, Y., Wang, H., Ma, X. & Mo, Y. 2020 Anti-clogging performance optimization for dentiform labyrinth emitters. *Irrigation Science* **38**, 275–285.

Zhai, G., Lu, M., Wang, H. & Xiang, H. 1999 Plugging of microirrigation system and its prevention. *Transactions of the CSAE* **15**, 144–147.

Zhangzhong, L., Yang, P., Ren, S., Liu, Y. & Li, Y. 2015 Flow characteristics and pressure-compensating mechanism of non-pressure-compensating drip irrigation emitters. *Irrigation and Drainage* **64**, 637–646.

Zhao, Z., Liping, L., Junhong, L., Chen, W. & Lichun, D. 2016 CFD simulation of concentrated-suspension flow and particle distribution in a microchannel. *Journal of Chemical Engineering of Chinese Universities* **30**, 341–348.

Zheng, Y. G., Yu, H., Jiang, S. L. & Yao, Z. M. 2008 Effect of the sea mud on erosion-corrosion behaviors of carbon steel and low alloy steel in 2.4% NaCl solution. *Wear* **264**, 1051–1058.

First received 2 April 2021; accepted in revised form 9 November 2021. Available online 24 November 2021